

Potential effectiveness of visible-light-driven Fe/TiO₂ photocatalysts for degradation of dyes contaminated wastewater and their antibacterial activity

Chonlada Dechakiatkrai Theerakarunwong^{a,*}, Onnicha Kaewthet^a, Sukon Phanichphant^b

^a Chemistry Program, Faculty of Science and Technology, Nakhon Sawan Rajabhat University, Nakhon Sawan 60000 Thailand

^b Material Science Research Center, Faculty of Science, Chiang Mai University, Chiang Mai 50200 Thailand

*Corresponding author, e-mail: chonlada.d@nsru.ac.th

Received 17 Jun 2022, Accepted 21 Mar 2023

Available online 15 May 2023

ABSTRACT: Synthetic dyes are utilized across a variety of industries and pose potential threats to water quality which, adversely, affects human health and environment. Photocatalysis is an effective technique for degrading organic pollutants in wastewater by converting photons of light energy to chemical energy by using superior semiconducting materials. Herein, we emphasized the significance of wastewater treatment by using a visible-light-sensitive photocatalyst obtained by doping Fe into TiO₂ for achieving high removal efficiency. According to the experimental results, photodegradation rate of the dye by 80% of 3% wt. Fe-doped TiO₂ with 20% v/v H₂O₂ addition was achieved in acidic media with three successive recycling runs. Moreover, total organic carbon (TOC) values indicated that the dye was nearly mineralized into CO₂ and water. This result may be related to the terephthalate (TPA) analysis, indicating that the amount of generated hydroxyl radicals increases via H₂O₂ addition. In addition, preliminary toxicological study was conducted focusing on contamination of Ti particles in selected plants after exposure to treated water. The antibacterial efficiency of the selected photocatalyst was further tested against Gram-positive and Gram-negative pathogenic bacterial strains. The results revealed that 3% wt. Fe-doped TiO₂ was highly efficient in inactivating *Escherichia coli* and *Staphylococcus aureus* after 3 h under visible light illumination. Overall, our results provided an alternative for an inexpensive, non-toxic, stable, efficient, reusable, and excellent catalytic performance of 3% wt. Fe-doped TiO₂ photocatalyst materials with significant tasks remained for future study, including dye contaminated wastewater treatment, bacterial growth inhibition and simultaneously solar harvesting.

KEYWORDS: Fe-doped TiO₂, dye, photocatalytic, wastewater, antibacterial activity

INTRODUCTION

Water is an essential resource for human life and ecosystem. Water pollution has emerged into one of the most serious environmental issues, which has a drastic negative impact on human health, animals and plants as a whole. With the rise in industrial production in Nakhon Sawan Province, Thailand, especially textile industries; hence, water pollution is considered as the main source of environmental pollution despite high transportation density and agricultural run-offs.

Synthetic dye is a complex organic compound used in industrial processes such as textile, cosmetic and painting industries. When the dye is discharged into aquatic environments, it is difficult to degrade and, directly or indirectly, causes serious damage to human health with a possibility of producing secondary pollution to the ecosystem. Therefore, it is of utmost importance to remove dyes in water resources. In order to solve water pollution problems, water based nanotechnology in detoxification using nanomaterials as photocatalysts has attracted great attention due to the performance of inexhaustible solar energy [1–3]. Thailand is a tropical country, with strong solar energy throughout the year. It is, therefore, worth taking a

benefit from the solar energy in the use of photochemical degradation/removal of organic contaminants in the environment.

TiO₂ is a photocatalyst mostly used to treat water pollution because of its high photoactivity and less toxicity to ecosystem [4, 5]. In the photodegradation application, the overwhelming majority of mechanisms rely on the reactive hydroxyl radical (OH[•]), which is the key oxidizing species to decompose pollutants and regenerate carbon dioxide and water as by-products [6]. Unfortunately, the TiO₂ catalyst efficiency is limited, as photons are absorbed only in the ultraviolet region, which captures less than 4% of the solar light [7, 8]. Moreover, its limited photocatalytic efficiency is due to other factors including the inactiveness under visible light [9].

In order to enhance the TiO₂ visible spectral region and retarding of electron/hole recombination (e⁻/h⁺) for practical applications, major efforts are devoted to expand the photo absorption of TiO₂ to a longer wavelength by doping TiO₂ with either metal iron or non-metallic elements. Besides, introduction of Fe dopant into TiO₂ lattice may allow the semiconductor substitute of lattice atoms to enter the lattice interstices of TiO₂, enhancing its photocatalytic activity under

direct sunlight. Doping TiO₂ with irons is found to be effective to alter the (e⁻/h⁺) pair recombination rate which shifts the absorption edge of TiO₂ towards the visible light region [10–13]. In addition, the reactive oxygen species (ROS) of Fe-doped TiO₂ nanoparticles, indicating their potent antibacterial ability, can be beneficially used as an inhibitor of bacterial growth in, for instance, mild and facile synthesis method, synthesis of weakly toxic catalysts and easily tunable surface, which play an important role in disinfection applications.

This research aimed to investigate the removal of dye contaminated wastewater in Nakhon Sawan Province, Thailand. Various parameters were studied to identify the effects on photodegradation activities of Fe-doped TiO₂ in a homemade photoreactor compared with natural solar light. The antibacterial activity of photocatalysts was also investigated. This proposed method was cost-effective and highly efficient in providing energy-saving source of light to drive photochemical reactions.

EXPERIMENTATIONS

Preparation of Fe-doped TiO₂

As-obtained anatase TiO₂ nanoparticles were synthesized and characterized in accordance with our previous studies, indicating that the 3% wt. Fe-doped TiO₂ nanoparticles had the best activity [12]. Titanium isopropoxide (Merck, Germany) was used as a precursor for the synthesis of TiO₂ nanosol, and Fe(III) acetyl acetonate (Sigma-Aldrich, USA) was used as an iron dopant; while absolute ethanol and nitric acid were used as solvents. Titanium isopropoxide was mixed with absolute ethanol and nitric acid for 1 h under stirring at 80 °C on a cellophane membrane placed in a beaker containing a mixture of ethanol, ammonia, and deionized water (molar ratio 1:1:10). The TiO₂ sol was washed with deionized water 3 times, then dried and impregnated by doping with 3%wt. Fe dopant before being calcined at 400 °C for 3 h.

Photodegradation test: factors impacting photocatalytic activity

Photoefficiency of Fe-doped TiO₂

The photocatalytic activities of 2000 mg/l as-obtained catalyst at the selected ratio of 3% wt. Fe-doped TiO₂ was conducted by discoloration under solar lamp irradiation of bromothymol blue (BB), congo red (CR) (Ajax Finechem, Australia) and alizarin yellow R (AYR) (Sigma-Aldrich) at the concentration of 5 μM of each dye. To achieve adsorption-desorption equilibrium, the lamp was switched off for 30 min, whereas the dye solution was stirred in the homemade photoreactor. The visible light illumination with an intensity of 15.0 w/m² was undertaken to initiate the photocatalytic reaction. During photomineralizations, 5 ml

suspension was taken at a time interval of 0.5 h up to 5 h to evaluate the dye concentration. The absorption spectra of each dye were determined by using UV-Vis spectrophotometer (UV-1280, Shimadzu, Japan). The 3% wt. Fe-doped TiO₂ was used as catalyst for all of the treatments [14, 15].

The maximum photo-efficiency obtained above was used to investigate the parameters affecting the photoactivity of TiO₂ nanocomposite. Three factors: initial concentration of organic pollutants, pH and H₂O₂, were taken into consideration.

For initial organic pollutant concentration, the solutions of individual dyes were investigated at concentrations of 1, 3, 5, 7 and 9 μM. For pH conditions, the pH of the reaction was adjusted using NaOH and HNO₃ to obtain pH of 4.2, 7.0 and 11.7. All sample solutions were measured in descending concentrations every 30 min for 5 h. For H₂O₂ addition, a given amount of TiO₂ nanocomposite was put into a beaker containing each dye at the desired concentration under dark conditions until the adsorption equilibrium was reached. Afterward, H₂O₂ was added to make 5, 10, 15 and 20% v/v solutions. The efficiency of photocatalytic activity of all samples was calculated, in descending concentrations every 30 min for 5 h, using Eq. (1):

$$\text{Efficiency} = \frac{C_0 - C}{C_0} \times 100 \quad (1)$$

where C₀ is the concentration at an initial time and C is the concentration at the certain illumination time (t). The concentration of dye is a function of irradiation time under visible light based on a calibration curve created by UV-visible spectroscopy.

Total organic carbon was analyzed using a total organic carbon analyzer (Analytik Jena multi-N/C 3100, Germany). By using TPA method, the hydroxyl radical formation in the presence of 3% wt. Fe-doped TiO₂ and 3% wt. Fe/TiO₂/H₂O₂ under UVLED irradiation was also studied.

Reusabilit

The study of reusability of Fe-doped TiO₂ nanocomposite was conducted by repetitive adsorbing and photodegrading of each dye. After the first use, the catalyst was centrifuged at 100 rpm for 5 min, and the catalyst powder was collected, washed three times with 10 ml ethanol under mechanical stirring for 15 min, and reused for dye absorption under the same conditions. The reusability and stability were also investigated by using FTIR analysis.

Photoactivity of Fe-doped TiO₂ for industrial wastewater

Fe-doped TiO₂ nanoparticles with the optimum ratio of H₂O₂ were used to investigate the photocatalytic performance of organic pollutants in contaminated wastewater. The solution was placed under solar

irradiation for 5 h (9 am–2 pm) with an average light intensity of 15 W. The light intensity was measured by Digital LUX Light Meter (TES-1339R, China) every 30 min. An aliquot (3 cm³) was taken and centrifuged before analyzing the absorption spectra of the dyes.

Toxicity to plants

Two different plants, an aquatic *Salvinia cucullata* Roxb. ex Bory and a semi-aquatic *Oryza sativa*, were used as plant models in the toxicity studies. The plants were grown in treated wastewater for 3 months, and all parts of the plants were investigated for existing Ti element using atomic absorption spectrometer (AAS, PinAAcle 900T, PerkinElmer, USA) every 30 days during the experimental period. Similarly, plants grown in distilled water were used as a control. Plant parts, i.e. leaves, stems and roots of the individual samples were randomly collected, immediately air-dried, and ground to powder. The powdered samples were digested in a nitric acid and hydrofluoric acid solution (5:3 by volume) for 15 min using a microwave-assisted instrument at 200 °C, 25 bars and 800 W. The final digested solution was diluted to 50 ml and subsequently subjected to analysis of the Ti content by AAS.

Photocatalytic antibacterial activity

The ability of Fe-doped TiO₂ photocatalyst under visible light irradiation was conducted using the suitable performing 3% wt. Fe-doped TiO₂ obtained from the dye decolorization experiment. The antibacterial effect of the selected photocatalyst was further investigated on total bacteria in the real dye wastewater. *E. coli* (ATCC 25922) and *S. aureus* (ATCC 25923) were chosen as model pathogens. One ml of *E. coli* or *S. aureus* suspension in PBS was mixed with serial dilutions of 3% wt. Fe-doped TiO₂ to achieve a final concentration of 10⁵ CFU/ml. The photocatalytic activity of the mixtures was evaluated in the photoreactor under visible illumination in triplicates.

RESULTS AND DISCUSSION

Characterization

The Fe-doped TiO₂ nanoparticles were spherical with about 20–50 nm in diameter (Fig. S1). As shown in Fig. S2, all diffraction peaks indicated that the particles were 100% anatase with no Fe(III) peak detected as they successfully entered the TiO₂ lattice [12, 16]. A surface area of 111 m²/g was also evaluated. In correspondence with our previous report, Fe(III) could introduce the new energy band structure as it acted as the co-doped TiO₂ catalyst to suppress electrons and holes. Hence, the red-shift phenomenon was achieved by Fe doping into TiO₂ lattice, as previously described by Theerakarunwong and Phanichphant [12] in 2018. Additionally, the small ionic radius of Fe(III) incorporated in the TiO₂ structure was in a good agreement with our previous report [12]. Possibly, this result

indicated that Fe(III) doping led to charge transfer transition between the Fe d electron and the CB of TiO₂ [10]. The bandgap value (E_{bg}) was 2.78 eV for Fe/TiO₂ and 3.20 eV for undoped TiO₂ (Fig. S3). The narrow bandgap of Fe/TiO₂ could be due to the presence of Fe(III) in the TiO₂ lattice. Besides, the change in E_{bg} value possibly derived active attributes under the visible region for Fe/TiO₂, while TiO₂ alone was only active under UV light. Moreover, the immobilization of Fe(III) affected the effectiveness of TiO₂ photocatalyst by generating a new energy level between VB and CB of TiO₂, resulting in a decrease in bandgap energy of the photocatalyst composites.

The FT-IR spectra demonstrated the evidence related to the functional groups existing in the nanocatalyst structure. The FT-IR spectra of as-prepared TiO₂ and Fe-doped TiO₂ were shown in Fig. S4. The transmittance bands at 2800–3600 and 1400–1600 cm⁻¹ were assigned to the stretching vibration of the –OH group attributed to the coordination of H₂O molecules adsorbed on the surface of TiO₂. In addition, the presence of the –OH functional group played a key role in enhancing photocatalytic activity by serving as a photogenerated charge carrier and, subsequently, leading to the formation of a number of hydroxyl radicals (OH[•]) [17]. While the absorption band at 400–800 cm⁻¹ indicates Ti–O and Ti–O–Ti bonds, the weak transmittance band at 2200–2400 cm⁻¹ was attributed to Ti–O–Fe vibration. The presence of a strong transmittance band between 600 cm⁻¹ and 800 cm⁻¹ exhibited the phase structure of anatase TiO₂.

Photoefficiency of Fe-doped TiO₂

The catalytic degradation of dye was carried out at the maximum UV-Vis absorption spectra of AYR, BB and CR. As expected, the maximum absorption peaks decreased as a function of time. Fig. 1(a) shows the high and stable removal efficiency of BB and CR at the of 210 min time interval of 60% and 51%, respectively; while the removal efficiency of AYR under the same condition was 33%. To understand the performance of photocatalysts, the oxidation reaction following a pseudo-first-order kinetic model with a kinetic rate constant of 0.0351 mg/l was investigated. Hence, $-\ln(C_t/C_0)$ versus time was used to calculate the reaction rate.

In the photocatalytic process, various concentrations of dye were determined to evaluate the optimum condition for Fe-doped TiO₂ photocatalytic reaction. The degradation rate reached about 80% for BB and CR, while 69% was observed for AYR (Fig. 1(b)). The results could be explained that an increase in pollutant concentration led to accumulation of the final products which inhibited the degradation process [18]. Moreover, increasing the concentration of dyes resulted in efficiency reduction despite the constant amount

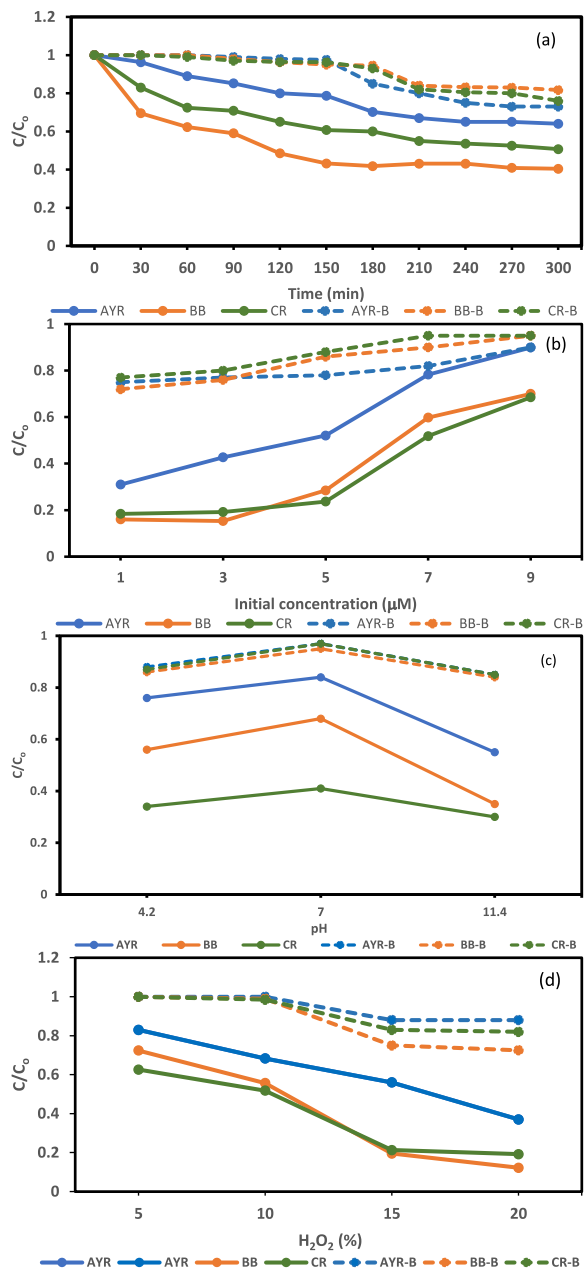


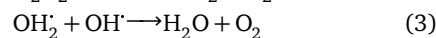
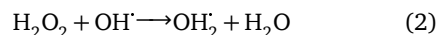
Fig. 1 Influence of: (a), time; (b), initial concentration of dye; (c), pH; and (d), % H₂O₂ on the degradation rate for the mineralization of AYR, BB and CR compared with the control groups AYR-B, BB-B and CR-B.

of Fe-doped TiO₂ and light intensity. This could be ascribed to an excess amount of dye, which inhibited light absorption of photocatalysts. By considering the Beer-Lambert law, the phenomenon resulted in less photons entering the solution, and thereby decreasing photocatalytic efficiency [9, 19]. Dye concentration was limited up to 5 μM as a higher concentration of dye induced an increase of organic species adsorption

by Fe-doped TiO₂ photocatalyst.

This research aimed to investigate the adsorption of anionic dye with Fe(III) modified TiO₂ in an aqueous solution of acidic, neutral and alkaline media. The surface charge of TiO₂ adsorbent was depended on the pH defined on the basis of the point of zero charge (pH_{pzc}) [20]. The findings, as shown in Fig. 1(c), indicated that the degradation rates for mineralization of AYR, BB and CR were under the influence of pH. The efficiency of degradation processes increased in acidic media when comparing among different pH conditions. The experimental PZC values for TiO₂ measured by acid-base potentiometric and mass titrations were 5.38 and 5.74, respectively [21]. At pH below TiO₂PZC, proton (H⁺) increased dramatically in strong acid media (pH 3.8). Consequently, the protonation of the OH groups at the surface of TiO₂ occurred and induced a number of positively charged adsorbent sites. Thus, acidic media favored the photodegradation of negatively charged dye in the presence of a positive charge TiO₂ surface. Conversely, at pH above TiO₂PZC, the suspension gained more OH groups, thus the anionic dye surface was surrounded by OH groups, causing an increase in the electrostatic repulsion and a decrease in efficiency of dye uptake [22, 23].

When H₂O₂ was added to the system, the removal ratios changed in the range of 81% to 92%. With the serial concentrations of H₂O₂, the highest removal efficiencies of AYR, BB and CR in 20% v/v H₂O₂ reached 63%, 88.8% and 81.8%, respectively; and 44%, 81.5% and 79.7%, respectively, in 15% v/v H₂O₂ (Fig. 1(d)). As a result, the addition of H₂O₂ tended to form OH[•] which served as primary oxidizing species in the photocatalytic process. The organic pollutant was oxidized via successive attacks by OH[•] radical. Moreover, the elevation of OH[•] radical was directly related to increasing photocatalytic efficiency due to the fact that H₂O₂ exhibited self-dissociation, resulting in the OH[•] increase [24]. However, the rising of H₂O₂ concentration did not impact the removal efficiency since its OH[•] radical scavenging effect could be explained as follows [25, 26]:



TOC analysis was used to assess mineralization of the target dyes at the desired irradiation time. In complete mineralization, the highly oxidizing species generated during the photocatalytic process led to attacking dye pollutants to release CO₂ and H₂O. However, by-products formation occurred during the degradation of organic pollutants. These compounds could be more toxic than parental contaminants. Therefore, TOC study was used to monitor the mineralization of dye and other by-products. It was worthwhile to note that 3% wt. Fe-doped TiO₂ photocatalyst gave lower TOC values. The results (Fig. S5) indicated a decrease

in TOC of BB and CR with decreased carbon content, meaning that dye molecules were decomposed to lower molecular weight compounds. Meanwhile, a higher TOC value obtained from AYR degradation indicated that more carbon was produced corresponded to the results obtained by photocatalytic activity of AYR by 3% wt. Fe-doped TiO₂ photocatalyst. For the first 30 min reaction time, a slow decline of TOC was observed and continued to decrease gradually until reaching a plateau at the reaction time of 210 min when the dye was nearly mineralized into CO₂ and H₂O [27]. In addition, the mineralization plateaus caused by 4.0–5.0 mg/l BB and CR dyes were much lower than that of AYR (about 9 mg/l), indicating that the stable products of BB and CR could be oxidized easily by Fe/TiO₂ photocatalysts compared with the AYR matrix.

The number of OH[•] radicals is known to be an important factor in pollutant photodegradation. To further clarify the effect of the amount of excited electron-hole pairs on the photocatalytic mineralization procedure, TPA analysis results were used to confirm the generation of OH[•] radicals. Two photocatalysts were investigated by TPA analysis as shown in Fig. S6. The intensity at the wavelength of 420 nm by TPA was found to increase with the reaction time up to 300 min, due to an increase in formation of OH[•] radicals during the photocatalytic degradation of organic dye with the increased reaction time under UVLED irradiation. Obviously, the amount of OH[•] radicals generated from 3% Fe/TiO₂/H₂O₂ photocatalysts was higher than that of 3% Fe/TiO₂ photocatalysts. These results confirmed that the amount of OH[•] radicals was the main reason for an effective process.

Recyclability

An ideal photocatalyst requires stability of photoactivity in which the efficacy does not only change during the reaction but maintains over the number of cycles. Although catalyst particles are not easy to use, they offer a highly photocatalytic activity due to their high specific surface area. In order to further verify the effectiveness of re-using the Fe-doped TiO₂ composite catalysts, the number of cycles in terms of activity stability was investigated. The results showed that the absorption spectra of the three dyes completely disappeared throughout the first three cycles of the reused catalysts with a degradation rate of more than 70%. However, the medium adsorption peaks resumed in the fourth cycle, suggesting that the efficiency of Fe-doped TiO₂ drastically declined (Fig. S7(a)). The reusability of the 3% wt. Fe-doped TiO₂ photocatalyst for the photodegradation of dyes was evaluated by using FT-IR analysis. The change in intensity of the functional group was monitored as a function of stability and reusability for Fe-doped TiO₂. As shown in Fig. S7(b), 3% wt. Fe-doped TiO₂ maintained band

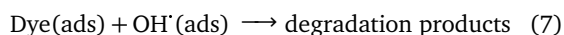
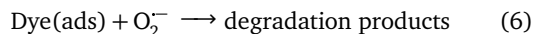
shapes of transmittance with no significant changes in intensity after three successive runs. However, the loss in recyclability was observed after three cycles, due to the block of the active sites by unremovable adsorbed dyes on the photocatalyst surface (Fig. S7(c) and (d)). The surface morphology of recycling Fe/TiO₂ composite catalysts showed remarkable changes. Confirmed by SEM images (Fig. S7(c)), porous and irregular morphology represented a large number of active sites available for dye adsorption up to the third cycle, while the agglomerated mesoporous framework was observed at the fourth cycle. This was possibly due to the excessive dye adsorption that saturated and covered on the surface of Fe/TiO₂. The same behavior was detected at cycle 5, which had dye molecules increased on the surface of Fe/TiO₂. The XRD patterns revealed the comparison between before and after dye adsorption. The main diffraction peaks of anatase TiO₂ was observed, indicating that the phase change of TiO₂ was not due to adsorption of dye molecules. However, the number of four small peaks around 27θ, 32θ, 42θ, and 54θ occurred during cycles 4–5. This finding suggested the loss of photo-efficiency. Other possible factors, such as time and pH, might be the cause of catalyst loss during photodegradation reaction, which led to reduction of the efficiency. To overcome these problems, further studies were required to understand the strong interaction between TiO₂ and various supporters and binders. Herein, its reusability over dye photodegradation was probably due to the formation of trapping sites by doping of Fe(III) into the TiO₂ lattice as previously discussed in the XPS section. Moreover, the emergence of this effect relied on the migration of photoactivated electrons from the binary Fe/TiO₂ heterojunction through the intimate interfacial contact between Fe(III) ions and Ti [26].

Applicable photocatalytic reaction mechanism

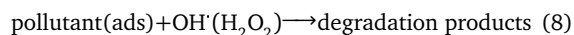
The applicable mechanism of photocatalytic reaction was presented in Fig. S8. When Fe/TiO₂ is irradiated with the light energy greater than its band gap energy, electrons are transferred from the VB to the CB, generating main reactions as follows: (1) charge carrier formation, (2) charge carrier recombination, (3) oxidation/reduction pathways by hole and excited electron, (4) reactive oxygen and hydroxyl species formation, and (5) trapping of a conduction band electron and hole. In our studies, the Fe(III) dopant had no effect on crystallinity of the TiO₂ framework. Therefore, the photo-efficiency depended on the activity of TiO₂ itself. However, Fe(III) dopant acted as the e⁻/h⁺ pair retardation in order to further improve the photo-efficiency, explained as follows:



Moreover, Fe^{3+} ions showed a positive standard reduction potential; therefore, the captured electron on the surface of TiO_2 could prevent the e^-/h^+ pair recombination. Furthermore, Fe^{3+} generated from the reaction caused by Fe^{2+} could release reactive species including O_2^- and OH^- [9]. The photo-degradation process occurred by the reaction between dye molecules and the reactive O_2^- and OH^- according to Eqs. (7)–(8):



Moreover, H_2O_2 addition with Fe/TiO_2 composite could promote OH^- radicals, as described in Eqs. (2)–(3), and further enhanced dye degradation as follows:



The effectiveness of photocatalysts in industrial wastewater

To investigate the photoactivity of Fe-doped TiO_2 in industrial wastewater, 2 sets of experiments was carried out under both synthetic illumination and solar stimulation. As shown in Table S1, samples from textile industry sites 1–5 were found to have removal efficiency ranges under synthetic illumination and solar stimulation of 76.15%–66.27% and 62.55%–51.38%, respectively. The average concentration of raw textile wastewater was 820 mg/l, which decreased to 160 mg/l after 3 h, corresponding to the average degradation percentage of 92.5%. The possible factors for low removal efficiency under synthetic solar light would be light energy insufficiency and lack of capability to penetrate in a high turbidity media. To confirm the results of comparison between 2 techniques, *F*-test was used to validate the 95% significance, with degree of freedom $n = 6$. From the results, $F_{\text{cal}}=1.1810 < F_{\text{cri}}=4.2839$, indicating that the difference was not significant at $p = 95\%$. Therefore, the degree of aggregation was induced by doping of Fe into the TiO_2 surface.

Toxicity of nanoparticles on plants

The TiO_2 nanoparticles were not found in all parts of plants, probably due to low concentration of Ti after the reaction. Ti could dissolve and release Ti(II) or Ti(III) in accordance with decreasing capacity of penetration through the cell membrane [28].

Photocatalytic disinfection

The evaluation of photocatalytic inhibition of 3% wt. Fe-doped TiO_2 against *E. coli* and *S. aureus* was conducted. The effect of contact time on the concentration of the selected pathogens indicated the reduction of cell viability of *E. coli* and *S. aureus* upon exposure to 3% wt. Fe-doped TiO_2 at different contact times through the plate count assay (Table 1). The present study showed that the highest positive result was found

Table 1 Counts of *E. coli* and *S. aureus* at the different contact time.

Population (log ₁₀ CFU/ml)	Contact time (min) [†] /(% reduction)			
	0	60	120	180
<i>E. coli</i>	7.01 ^a (–)	3.55 ^b (41.3%)	2.10 ^{bc} (52.6%)	1.07 ^c (67.5%)
<i>S. aureus</i>	7.25 ^a (–)	4.76 ^b (38.3%)	3.87 ^b (43.5%)	4.01 ^b (45.8%)
Control + light				
<i>E. coli</i>	7.01 ^a (–)	6.65 ^b (12.23%)	5.05 ^b (21.1%)	4.07 ^b (34.6%)
<i>S. aureus</i>	7.25 ^a (–)	6.54 ^b (11.5%)	5.45 ^b (21.4%)	5.10 ^b (24.7%)
Control + dark				
<i>E. coli</i>	7.01 ^a (–)	7.01 ^a (–)	7.01 ^a (–)	7.01 ^a (–)
<i>S. aureus</i>	7.25 ^a (–)	7.25 ^a (–)	7.25 ^a (–)	7.25 ^a (–)

[†] Different lower-case letters show significant differences ($p < 0.05$) between contact time within same bacterial strain.

when tested with *E. coli* (67.5%), followed by *S. aureus* (45.8%) under the intensity of 10.5 W visible light. The control experiments without addition of photocatalysts under light/dark conditions were also evaluated. From the results, no reduction was detected for the control group without illumination; whilst, the inhibition of bacterial growth was found under illumination treatment. In comparison to the control group, the reduction of microbial survival treated with 3% wt. Fe-doped TiO_2 under photocatalysis systems decreased significantly ($p \leq 0.05$). The 3% wt. Fe-doped TiO_2 generated intracellular reactive oxygen species (ROS) and malondialdehyde, which influenced the antibacterial capabilities. These ROS adhered to the bacteria's surface and further oxidized cell walls then caused damages to morphology of the cell membrane. Simultaneous shrinkage of the cells led to leakage of intracellular fluid and cell death [29,30]. Gram-negative *E. coli* is known to have a thin peptidoglycan layer with an outer lipid membrane, while *S. aureus* is Gram-positive with a thick peptidoglycan layer without an outer lipid membrane. ROS released during the photocatalytic reaction had significantly greater destructive effects on *E. coli* cells than negative charge *S. aureus* cells [31]. Moreover, the positively charged modified Fe-doped TiO_2 could increase a greater affinity of the negative charge of *E. coli* cell membrane, leading to the increase in efficiency. Hence, antibacterial effects against Fe-doped TiO_2 photocatalyst offered considerably more advantages over traditional antibacterial agents.

CONCLUSION

It could be concluded from the study of Fe-doped TiO₂ nanocatalyst synthesis that these nanomaterials had immense reactive potential to treat organic pollutant contaminated wastewater. Under UV irradiation, the absorption of TiO₂ was limited. Fe loading into TiO₂ preserved the value for real solar system purposes due to the increase in the absorption towards longer wavelength, which raised the possibility to generate electron-hole pair and further enhanced the removal reaction. For dye degradation, the doping of Fe(III) notably improved dye removal rates due to the increases of OH[•] radicals created. Moreover, the photocatalytic performance was evaluated to identify antibacterial activities against *E. coli* and *S. aureus* under visible light irradiation. The photocatalytic inhibition of both bacteria was observed. Lastly, our concerns were on the risks of exposure and toxicity of nanomaterials through the recurrent use of treated wastewater in planting. The results of our experiments showed that there was no presence of Ti residue in all parts of selected plants. However, differences in size, concentration of nanomaterial, treated wastewater, and plant species may cause varied interactions. Therefore, further studies, in particular, on the mechanisms of interaction between the nanomaterials and living cells are required.

Appendix A. Supplementary data

Supplementary data associated with this article can be found at <http://dx.doi.org/10.2306/scienceasia1513-1874.2023.xxx>.

Acknowledgements: The authors acknowledge the support of Chemistry Program, Faculty of Science and Technology, Nakhon Sawan Rajabhat University for the use of its facilities.

REFERENCES

- Choi H, Al-Abed SR, Dionysiou DD, Stathatos E, Lianos P (2010) Chapter 8 TiO₂-based advanced oxidation nanotechnologies for water purification and reuse. *Sustain Sci Eng* **2**, 229–254.
- Jiang L, Wang Y, Feng C (2012) Application of photocatalytic technology in environmental safety. *Procedia Eng* **45**, 993–997.
- Byrne C, Subramanian G, Pillai SC (2018) Recent advances in photocatalysis for environmental applications. *J Environ Chem Eng* **6**, 3531–3555.
- Haque MM, Muneer M (2007) TiO₂-mediated photocatalytic degradation of a textile dye derivative, bromothymol blue in aqueous suspensions. *Dyes Pigm* **75**, 443–448.
- Somsongul V, Chirawatkul P, Kongmark C (2021) Enhanced visible response of TiO₂ nanoparticles by natural dyes. *ScienceAsia* **47S**, 69–75.
- Nasirian M, Mehrvar M (2018) Photocatalytic degradation of aqueous methyl orange using nitrogen-doped TiO₂ photocatalyst prepared by novel method of ultraviolet-assisted thermal synthesis. *J Environ Sci* **66**, 81–93.
- Pal NK, Kryschi C (2016) Improved photocatalytic activity of gold decorated differently doped TiO₂ nanoparticles: A comparative study. *Chemosphere* **144**, 1655–1664.
- Sompech S, Jittabut P, Thaomola S, Audtarat S, Charee P, Dasri T (2021) Localized surface plasmon resonance for improving optical absorption in core-shell Ag@TiO₂ nanoparticles. *ScienceAsia* **47**, 340–346.
- Dara M, Hassanpour M, Alshamsi HA, Baladi M, Salavati-Niasari M (2021) Green sol-gel auto combustion synthesis and characterization of double perovskite Tb₂ZnMnO₆ nanoparticles and a brief study of photocatalytic activity. *RSC Adv* **11**, 8228–8238.
- Theerakarunwong CD, Chuaychai W, Phanichphant S (2021) Iron decorated n-TiO₂ film with enhanced photocatalytic activity under visible irradiation. *Songklanakarin J Sci Technol* **43**, 660–666.
- Zou M, Xiong F, Ganeshraja AS, Wang C, Thomas T, Yang M (2017) Visible light photocatalysts (Fe,N):TiO₂ from ammonothermally processed, solvothermal self-assembly derived Fe-TiO₂ mesoporous microspheres. *Mater Chem Phys* **195**, 259–267.
- Theerakarunwong DC, Phanichphant S (2018) Visible-light-induced photocatalytic degradation of PAH-contaminated soil and their pathways by Fe-doped TiO₂ nanocatalyst. *Water Air Soil Pollut* **229**, 291.
- Theerakarunwong DC, Phothi R (2018) Community refinery wastewater photodegradation by Fe-doped TiO₂ film. *Water Air Soil Pollut* **229**, 231.
- Theerakarunwong DC, Phanichphant S (2015) Photocatalytic degradation of aromatic pollutants in aqueous solution over TiO₂ catalyst. *Chiang Mai J Sci* **42**, 939–945.
- Theerakarunwong DC, Phanichphant S (2016) Photoremediation of phenanthrene contaminated soil under visible light irradiation. *Chiang Mai J Sci* **43**, 845–850.
- Khalilzadeh A, Shariati A (2018) Photoreduction of CO₂ over heterogeneous modified TiO₂ nanoparticles under visible light irradiation: Synthesis, process and kinetic study. *Sol Energy* **164**, 251–261.
- Ali T, Tripathi P, Azam A, Raza W, Ahmed AS, Ahmed A, Muneer M (2016) Photocatalytic performance of Fe-doped TiO₂ nanoparticles under visible-light irradiation. *Mater Res Express* **4**, 015022.
- Nath RK, Zain MFM, Jamil M (2016) An environment-friendly solution for indoor air purification by using renewable photocatalysts in concrete. *Renew Sust Energ Rev* **62**, 1184–1194.
- Khan MM, García ME, Javed M, Kubacka A, Caudillo-Flores U, Halim SA, Khan A, Al-Harrasi A, et al (2021) Synthesis, characterization, and photocatalytic, bactericidal, and molecular docking analysis of Cu-Fe/TiO₂ photocatalysts: Influence of metallic impurities and calcination temperature on charge recombination. *ACS Omega* **6**, 26108–26118.
- Hussein FH (2012) Photochemical treatments of textile industrial wastewater. *Asian J Chem* **24**, 5427–5434.
- Miyittah MK, Tsyawo FW, Kumah KK, Stanley CD, Rechigl JE (2016) Suitability of two methods for determination of point of zero charge (PZC) of adsorbents in soils. *Commun Soil Sci Plant Anal* **47**, 101–111.
- Alam MS, Khanom R, Rahman MA (2015) Removal of Congo red dye from industrial wastewater by untreated sawdust. *Am J Environ Prot* **4**, 207–213.

23. Al-Rubayee WT, Abdul-Rasheed OE, Ali NM (2016) Preparation of a modified nanoalumina sorbent for the removal of alizarin yellow R and methylene blue dyes from aqueous solutions. *J Chem* **2016**, 4683859.
24. Mancuso A, Sacco O, Vaiano V, Bonelli B, Esposito S, Freyria FS, Blangett N, Sannino D (2021) Visible light-driven photocatalytic activity and kinetics of Fe-Doped TiO₂ prepared by a three-block copolymer templating approach. *Materials* **14**, 3105.
25. Tayade RJ, Natarajan TS, Bajai HC (2009) Photocatalytic degradation of methylene blue dye using ultraviolet light emitting diodes. *Ind Eng Chem Res* **48**, 10262–10267.
26. Chowdhury M, Shoko S, Cummings F, Fester V, Ojumu TV (2017) Charge transfer between biogenic jarosite derived Fe³⁺ and TiO₂ enhances visible light photocatalytic activity of TiO₂. *J Environ Sci* **54**, 256–267.
27. Zhang Q, Li C, Li T (2012) Rapid photocatalytic degradation of methylene blue under high photon flux UV irradiation Characteristics and comparison with routine low photon flux. *Int J Photoenergy* **2012**, 7.
28. Chichiricò G, Poma A (2015) Penetration and toxicity of nanomaterials in higher plants. *Nanomaterials* **5**, 851–873.
29. Wang W, Huang G, Yu JY, Wong PK (2015) Advances in photocatalytic disinfection of bacteria: Development of photocatalysts and mechanisms. *J Environ Sci* **34**, 232–247.
30. Rashki S, Alshamsi HA, Amiri O, Safardoust-Hojaghan H, Salavati-Niasari M, Nazari-Alam A, Khaledi A (2021) Eco-friendly green synthesis of ZnO/GQD nanocomposites using *Protopermeliosis muralis* extract for their antibacterial and antibiofilm activity. *J Mol Liq* **335**, 116195.
31. Hou J, Wang L, Wang C, Zhang S, Liu H, Li S, Wang X (2019) Toxicity and mechanisms of action of titanium dioxide nanoparticles in living organisms. *J Environ Sci* **75**, 40–53.

Appendix A. Supplementary data

Table S1 Efficiency of dye removal under synthetic and solar lights from different textile sites in Nakhon Sawan Province.

Sample site	% Removal rate \pm SD	
	Synthetic light (15 W)	Solar light (4.8 W)
Site 1	76.15 \pm 1.50	62.55 \pm 2.30
Site 2	70.50 \pm 2.00	50.65 \pm 3.50
Site 3	67.43 \pm 3.50	56.45 \pm 3.50
Site 4	68.50 \pm 2.43	55.20 \pm 3.28
Site 5	66.27 \pm 1.07	51.38 \pm 2.74

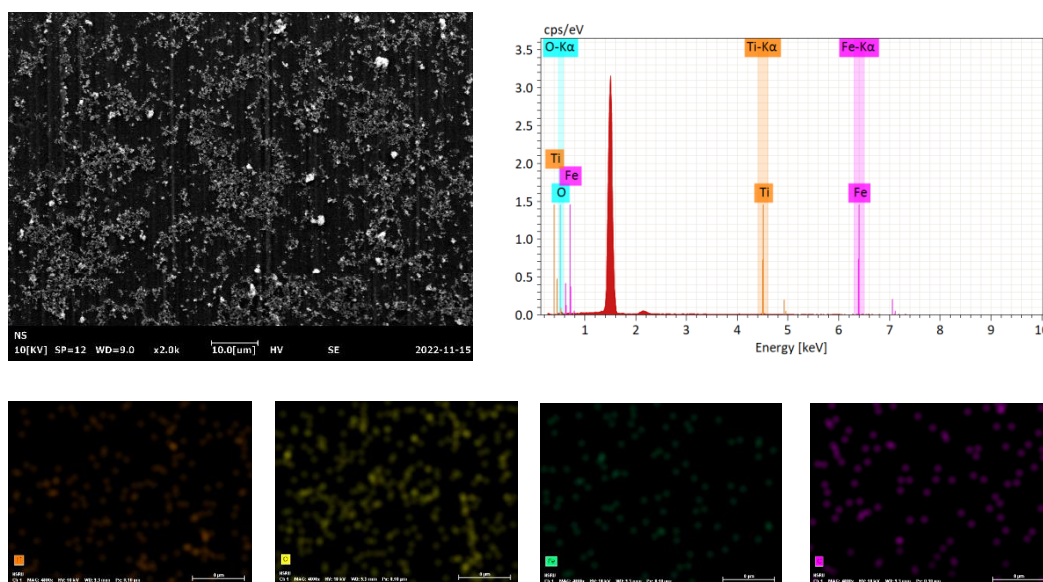


Fig. S1 SEM and EDS analyses of Fe-doped TiO₂.

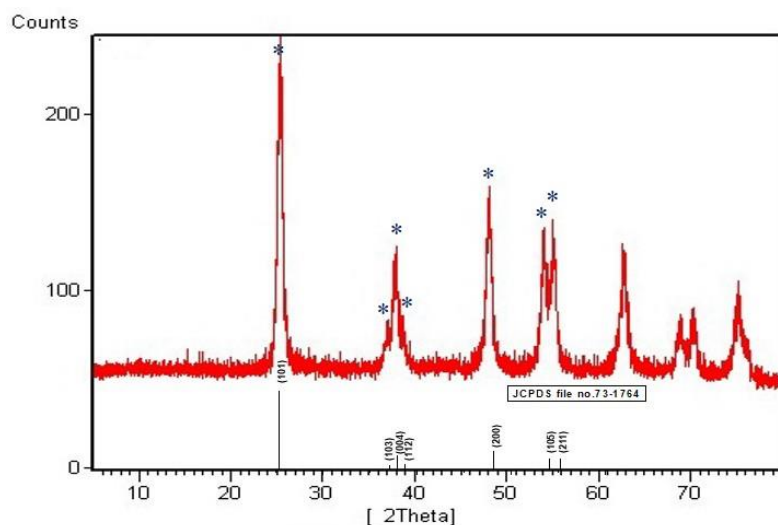


Fig. S2 XRD pattern of 3% wt. Fe-doped TiO₂.

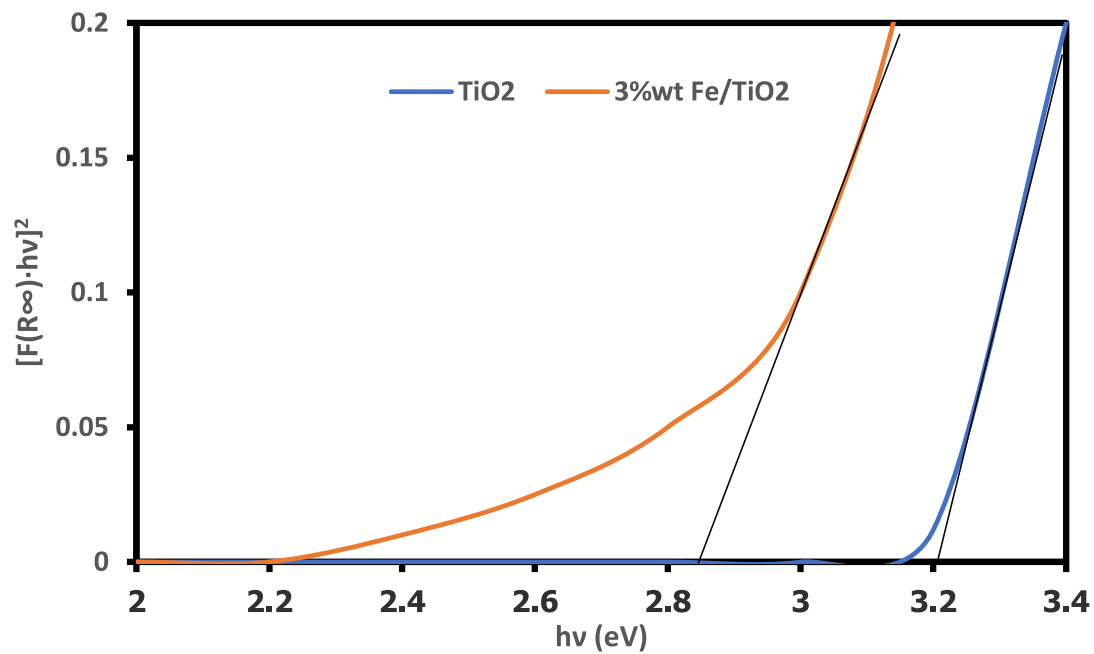


Fig. S3 Bandgap energy of bare TiO_2 and 3% wt. Fe-doped TiO_2 .

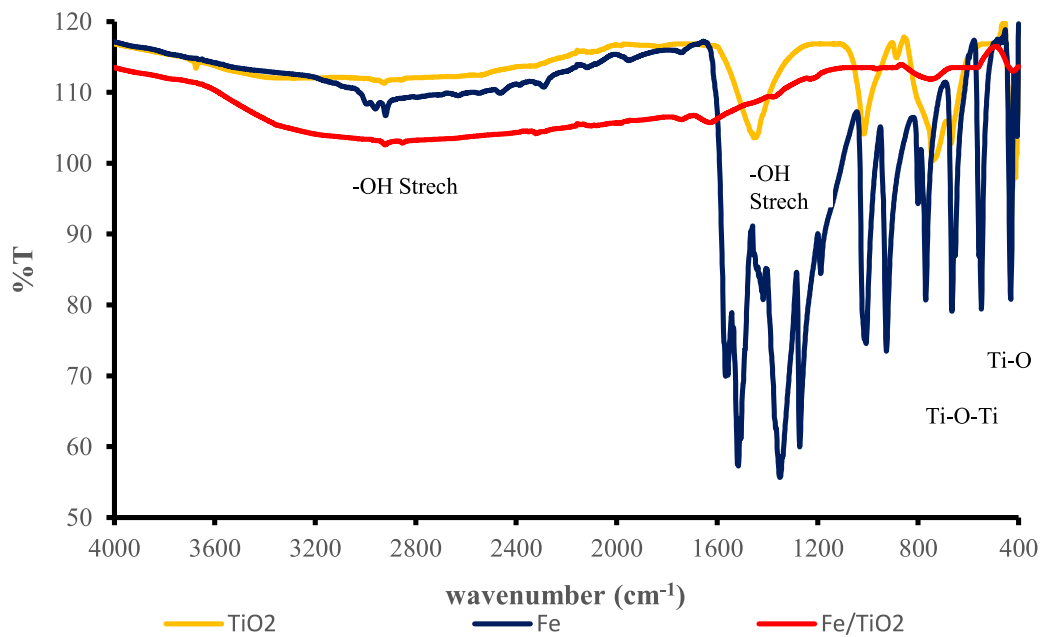


Fig. S4 FT-IR spectra of TiO_2 , Fe and 3% wt. Fe-doped TiO_2 .

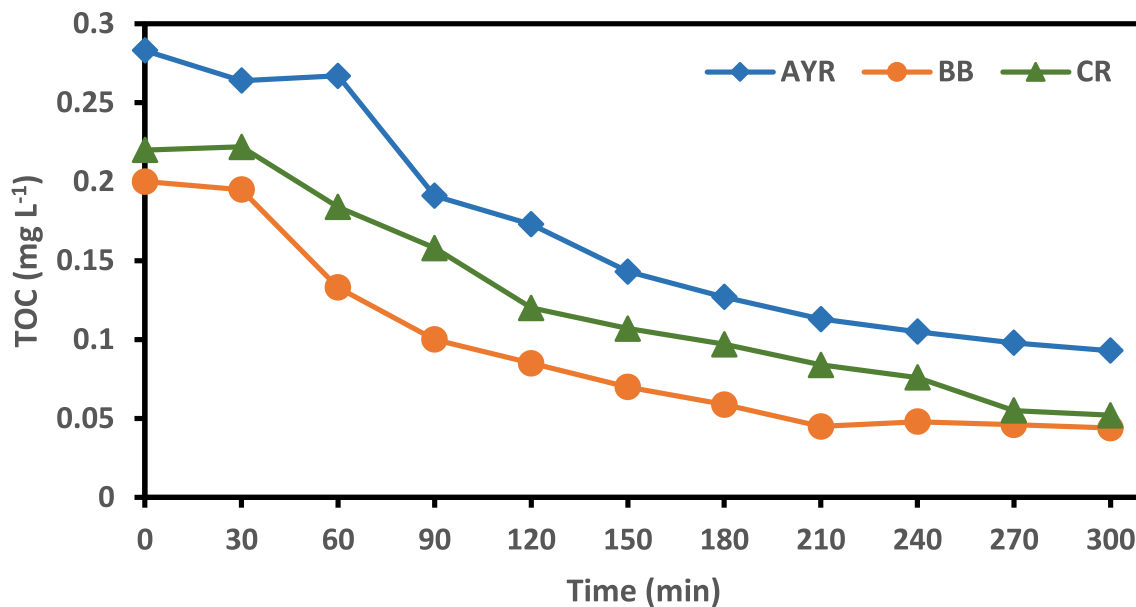


Fig. S5 Relationship between TOC removal efficiency and reaction time by 3% wt. Fe-doped TiO₂ with 20% v/v H₂O₂, pH 3.8 and dye initial concentration of 10 mg/l.

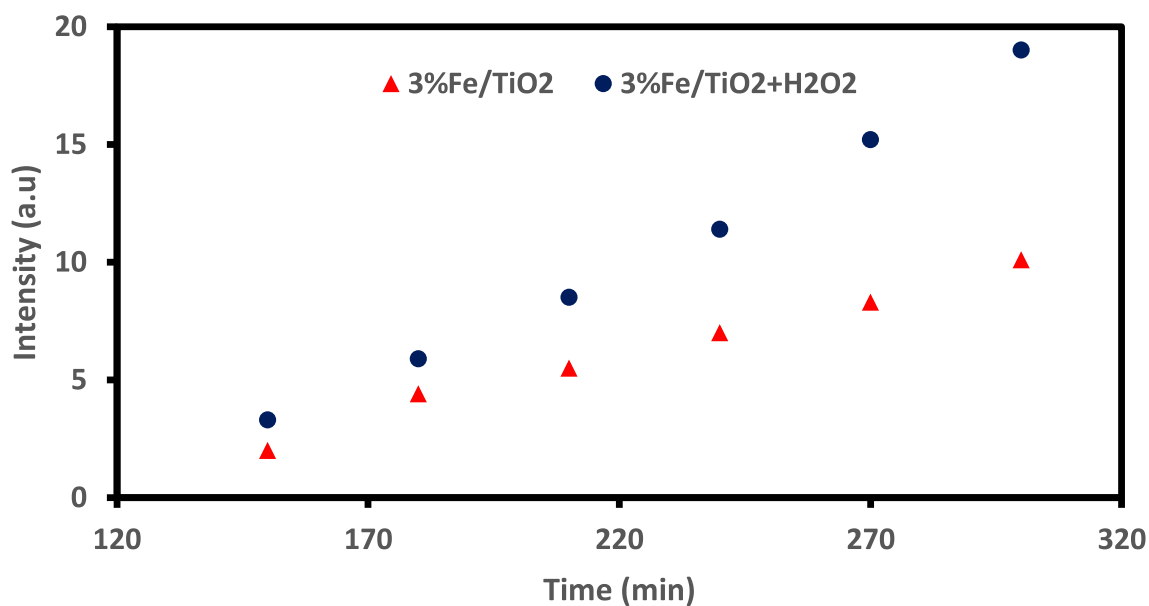


Fig. S6 TPA analysis of 3% Fe/TiO₂ photocatalysts and 3% Fe/TiO₂H₂O₂ photocatalysts at the maximum wavelength of 420 nm.

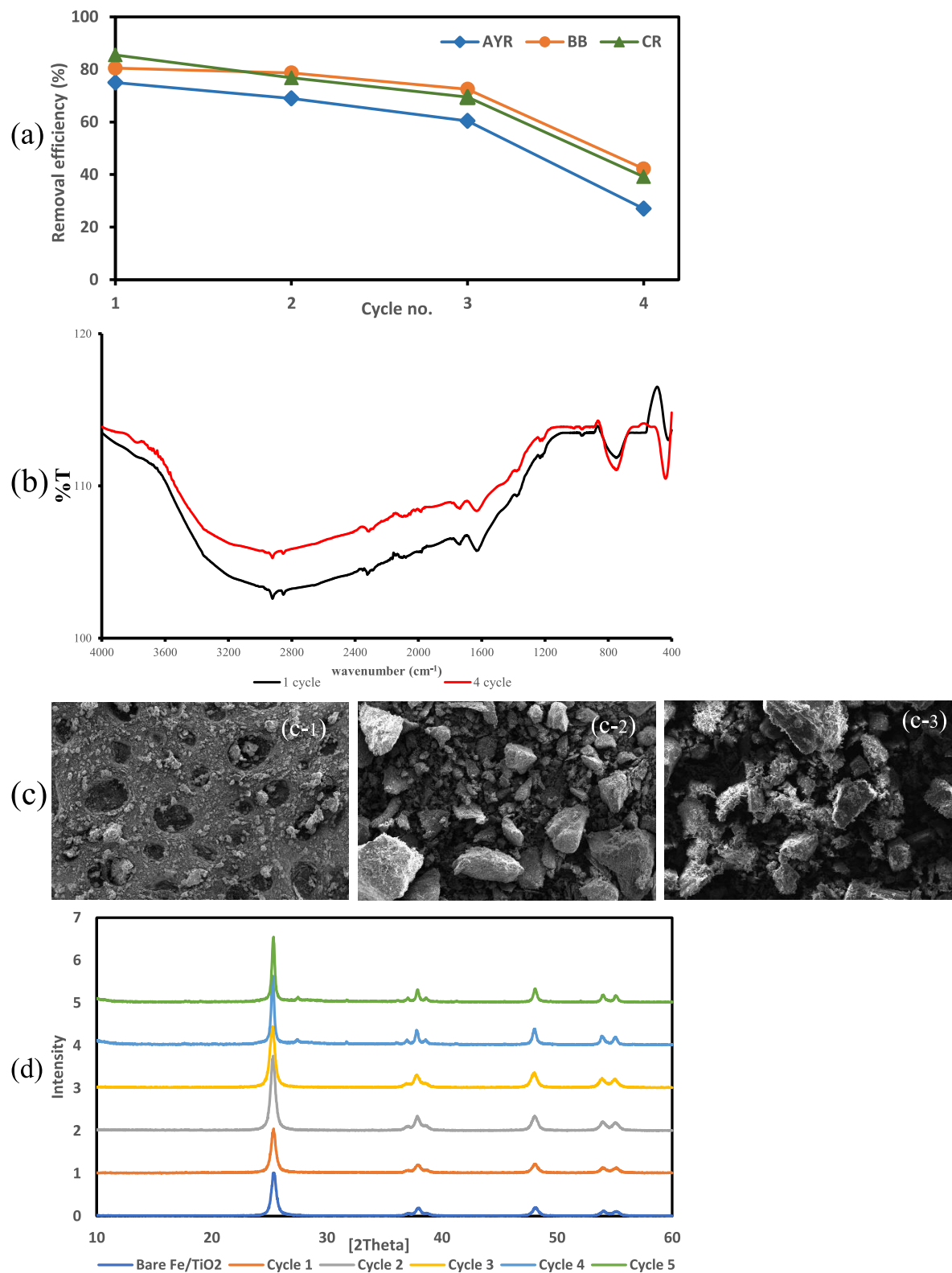


Fig. S7 Recyclability on: (a), the removal efficiency of before and after dye adsorption of adsorbent Fe/TiO₂; (b), FT-IR spectra of recycling 3% wt. Fe-doped TiO₂; (c), SEM images of adsorbent material {(c-1) cycle 3 (c-2) cycle 4 (c-3) cycle 5}; and (d), XRD patterns of bare Fe/TiO₂ before and after dye adsorption of adsorbent Fe/TiO₂ (cycles 1–5).

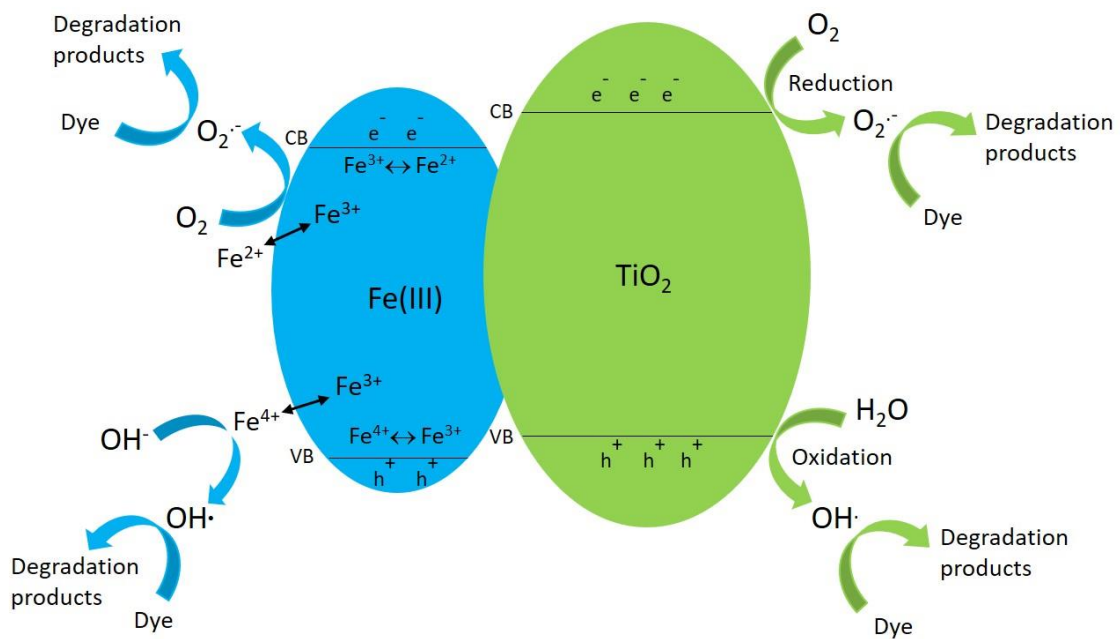


Fig. S8 Possible photocatalytic reaction mechanism of Fe/TiO₂ photocatalyst with dyes.